

# Wafer-Scale Single-Crystal Monolayer Graphene Grown Directly on Insulating Substrates

**Junzhu Li**

King Abdullah University of Science and Technology

**Mingguang Chen**

Physical Science and Engineering Division, King Abdullah University of Science and Technology, Thuwal 23955-6900, Saudi Arabia.

**Abdus Samad**

King Abdullah University of Science and Technology

**Haocong Dong**

Eleven-dimensional Nanomaterial Research Institute

**Avijeet Ray**

King Abdullah University of Science and Technology

**Junwei Zhang**

Key Laboratory for Magnetism and Magnetic Materials of Ministry of Education, Lanzhou University, Lanzhou 730000, People's Republic of China

**Xiaochuan Jiang**

Xiamen University

**Udo Schwingenschlogl**

King Abdullah University of Science and Technology

**Jari Domke**

Institute of Solid State Physics(IFK), Friedrich Schiller University Jena, Helmholtzweg 5, 7743 Jena, Germany

**Cailing Chen**

Physical Science and Engineering Division, King Abdullah University of Science and Technology (KAUST), Thuwal 23955-6900, Saudi Arabia

**Yu Han**

Physical Science and Engineering Division, King Abdullah University of Science and Technology (KAUST), Thuwal 23955-6900, Saudi Arabia

**Torsten Fritz**

Institute of Solid State Physics(IFK), Friedrich Schiller University Jena, Helmholtzweg 5, 7743 Jena, Germany

**Bo Tian** (✉ [bo.tian@kaust.edu.sa](mailto:bo.tian@kaust.edu.sa))

King Abdullah University of Science and Technology <https://orcid.org/0000-0002-1575-0491>

**Xixiang Zhang** (✉ [xixiang.zhang@kaust.edu.sa](mailto:xixiang.zhang@kaust.edu.sa))

## Article

**Keywords:** single-crystal graphene, MPE-CVD, metal catalysis

**Posted Date:** May 17th, 2021

**DOI:** <https://doi.org/10.21203/rs.3.rs-95262/v1>

**License:**  This work is licensed under a Creative Commons Attribution 4.0 International License.

[Read Full License](#)

---

**Version of Record:** A version of this preprint was published at Nature Materials on January 20th, 2022. See the published version at <https://doi.org/10.1038/s41563-021-01174-1>.

1 **Wafer-Scale Single-Crystal Monolayer Graphene Grown Directly on**  
2 **Insulating Substrates**

3 Junzhu Li<sup>1,2</sup>, Mingguang Chen<sup>1</sup>, Abdus Samad<sup>1</sup>, Haocong Dong<sup>1,2</sup>, Avijeet Ray<sup>1</sup>, Junwei Zhang<sup>3</sup>,  
4 Xiaochuan Jiang<sup>2,4</sup>, Udo Schwingenschlögl<sup>1</sup>, Jari Domke<sup>5</sup>, Cailing Chen<sup>1</sup>, Yu Han<sup>1</sup>, Torsten  
5 Fritz<sup>5</sup>, Bo Tian<sup>1,2\*</sup>, Xixiang Zhang<sup>1\*</sup>

6 <sup>1</sup>Physical Science and Engineering Division, King Abdullah University of Science and  
7 Technology (KAUST), Thuwal 23955-6900, Saudi Arabia.

8 <sup>2</sup>Eleven-dimensional Nanomaterial Research Institute, Xiamen 361005, China.

9 <sup>3</sup>Key Laboratory of Magnetism and Magnetic Materials of Ministry of Education, Lanzhou  
10 University, Lanzhou 730000, China.

11 <sup>4</sup>Department of Physics, Xiamen University, Xiamen 361005, China.

12 <sup>5</sup>Institute of Solid State Physics (IFK), Friedrich Schiller University Jena, Helmholtzweg 5,  
13 07743 Jena, Germany

14 \*e-mail: bo.tian@kaust.edu.sa; xixiang.zhang@kaust.edu.sa

1 **Currently, the direct synthesis of inch-scale single-crystal graphene on insulating**  
2 **substrates is limited by the lack of metal catalysis, suitable crystallization conditions, and**  
3 **self-limiting growth mechanisms. In this study, we investigated the direct growth of**  
4 **adlayer-free ultra-flat wafer-scale single-crystal monolayer graphene on insulating**  
5 **substrates by the multi-cycle plasma-etching-assisted chemical vapor deposition (MPE-**  
6 **CVD) method. Firstly, an angstrom-scale growth nanochamber was created by fabricating**  
7 **single-crystal Cu(111) foils on Al<sub>2</sub>O<sub>3</sub>(0001) substrates. Graphene was then directly**  
8 **synthesized at the interface between Cu(111) and Al<sub>2</sub>O<sub>3</sub>(0001) by MPE-CVD. After growth,**  
9 **the Cu(111) foil was detached using a liquid-nitrogen-assisted separation method, and the**  
10 **ultra-high-quality single-crystal graphene film was experimentally achieved on**  
11 **Al<sub>2</sub>O<sub>3</sub>(0001). This work breaks the bottleneck in the direct synthesis of single-crystal**  
12 **monolayer graphene on insulating substrates and paves the way for next-generation**  
13 **carbon-based atomic electronics and semiconductor nanodevices.**

1 As a pioneer two-dimensional (2D) nanomaterial, graphene has attracted considerable  
2 interest in the science community<sup>1,2</sup>. Owing to its remarkable physical-chemical properties, the  
3 application of graphene is expected to bring technological breakthroughs in next-generation  
4 semiconductor nanodevices<sup>3</sup>. However, due to the limitations of graphene synthesis techniques,  
5 the prospective value and theoretically predicted properties of graphene have not yet been  
6 realized. In recent years, the discovery of superconductivity in magic-angle graphene devices has  
7 renewed the interest in graphene and its numerous attractive features<sup>4,5</sup>. Chemical vapor  
8 deposition (CVD), which involves self-limiting growth mechanisms by the Cu-catalyzed  
9 cracking of methane, is the most widely used synthetic method to grow high-quality large-scale  
10 graphene<sup>6</sup>. However, the conventional Cu-substrate CVD-grown graphene has inevitable issues  
11 such as electron scattering at grain boundaries, wrinkles, and adlayers, that significantly affect its  
12 electronic properties, thus limiting its application<sup>7</sup>. To date, the majority of laboratory-made  
13 graphene nanodevices are still fabricated on manually exfoliated small graphene flakes because  
14 of their superior crystal quality compared with traditional CVD-grown graphene. In light of this,  
15 a synthesis method of large-area ultra-high-quality CVD-grown graphene is urgently needed to  
16 translate the ideal properties of graphene to practical applications in the scientific research and  
17 industry.

18 To improve the quality of CVD-grown graphene, various strategies have been explored<sup>8-</sup>  
19 <sup>10</sup>, including the synthesis of (i) single-crystal graphene by single-nuclei preferential growth<sup>11</sup>,  
20 (ii) adlayer-free graphene by Cu-substrate carbon-removal pretreatment<sup>12</sup>, and (iii) ultra-flat  
21 graphene by proton penetration<sup>13</sup>. These strategies resolved various problems related to  
22 conventional Cu-substrate CVD growth, leading to almost perfect graphene. However, as a  
23 metallic 2D material, graphene must be transferred to insulating substrates for application in

1 nanodevices, which unavoidably introduce secondary contaminations, cracks, folds, and  
2 unexpected doping<sup>14</sup>. Hence, a more straightforward strategy was proposed through the direct  
3 CVD growth of graphene on insulating substrates. Some attempts have been made such as  
4 oxygen-assisted growth<sup>15</sup>, molten-glass-substrate synthesis<sup>16</sup>, metal-substrate carbon  
5 dissolution<sup>17</sup>, carbon diffusion through Cu grain boundaries<sup>18</sup>, Cu-vapor-assisted CVD process<sup>19</sup>,  
6 and high-temperature metal-free H<sub>2</sub>-etched assisted growth<sup>20</sup>. These methods enable the direct  
7 growth of polycrystalline graphene layers on insulating substrates. However, due to the lack of  
8 layer-controlled mechanisms, lattice-matching epitaxy conditions, relatively low speed ratio of  
9 growth/etch, and strong interaction with insulating substrates, graphene with extremely small  
10 domain sizes, poor crystal qualities, and an uncontrolled number of layers was obtained, which  
11 limited its performance in practical nanodevices. Therefore, the direct synthesis of high-quality  
12 single-crystal graphene on insulating substrates remains a critical task.

13 In our study, we achieved the direct growth of a layer-free ultra-flat wafer-scale single-  
14 crystal monolayer graphene on insulating substrates by the multi-cycle plasma-etching-assisted  
15 CVD (MPE-CVD) growth method. First, wafer-scale single-crystal Cu(111) foils were  
16 synthesized on Al<sub>2</sub>O<sub>3</sub>(0001) from commercial polycrystalline Cu foils (25 μm thick) by a long-  
17 term annealing-driven phase-transition process. An angstrom-scale-thick superlattice-potential-  
18 distributed growth nanochamber (ASG nanochamber) was formed at the interface of the top  
19 Cu(111) foil and bottom Al<sub>2</sub>O<sub>3</sub>(0001) substrate. In this ASG nanochamber, the ultra-high-quality  
20 single-crystal graphene film was synthesized through MPE-CVD growth. The Cu(111) foil was  
21 easily detached after the growth process by a liquid-nitrogen-assisted extreme-temperature-  
22 difference separation method.

## Preparation of large-scale single-crystal Cu(111) on Al<sub>2</sub>O<sub>3</sub>(0001)

The structures and properties of the substrates significantly affect the crystal orientation and domain symmetry of as-grown 2D materials; therefore, significant effort has been devoted to modifying substrates<sup>21,22</sup>. Cu(111) is considered as an ideal substrate for the synthesis of single-crystal 2D materials with triangular and hexagonal symmetries such as h-BN ( $C_{3v}$ ) and graphene ( $C_{6v}$ )<sup>23,24</sup>. Hence, the fabrication of large-scale single-crystal Cu foils is the key for the synthesis of high-quality wafer-scale 2D materials. In a previous study, the single-crystal Cu(111) foil was fabricated via contact-free annealing<sup>25</sup>. Inspired by this work, we produced 2-inch single-crystal Cu(111) foils on Al<sub>2</sub>O<sub>3</sub>(0001) substrates from commercial polycrystalline Cu foils by long-term near-melting-temperature annealing under a hydrogen–argon atmosphere, taking advantage of lattice matching and crystal symmetry ( $C_{6v}$ ).

First, the as-received polycrystalline Cu foil was electrochemically polished and laminated atop an O<sub>2</sub>-plasma-treated Al<sub>2</sub>O<sub>3</sub>(0001) substrate, forming a Cu/Al<sub>2</sub>O<sub>3</sub> heterostructure, which was then placed in a CVD system for long-term high-temperature annealing under specific conditions (Supplementary Fig. 1). According to the energy distribution, Cu(111) was the most stable crystal with the lowest steady-state energy on the Al<sub>2</sub>O<sub>3</sub>(0001) substrate compared with Cu(110) and Cu(100) crystals (Fig. 1a). Therefore, during annealing, the differently oriented crystals gradually relaxed and transformed into Cu(111) with the lowest stacking energy and formed a single crystal to reduce the grain boundary energy (Fig. 1b). To investigate the Cu crystalline phase change with annealing time, a series of time-dependent experiments was conducted. The data measured for 10 samples in each experiment revealed the gradual increase in the grain size of the Cu(111) crystal with annealing time, eventually covering the entire 100 mm<sup>2</sup> Al<sub>2</sub>O<sub>3</sub>(0001) substrate (Fig. 1c). To more straightforwardly observe the phase transformation,

1 oxidization treatment was conducted on Cu foils owing to the change in the color of copper  
2 oxide ( $\text{CuO}_x$ ) depending on Cu crystal orientations<sup>26</sup> (Supplementary Fig. 2). In comparison, the  
3 phase transformations were not observed on other substrates, such as quartz,  $\text{Al}_2\text{O}_3(10-10)$ , and  
4  $\text{Al}_2\text{O}_3(11-20)$  (Supplementary Fig. 3). Furthermore, depending on the spatial uniformity of this  
5 phase transformation, we successfully fabricated 2-inch single-crystal Cu(111) foils on  
6  $\text{Al}_2\text{O}_3(0001)$  wafers. Optical microscopic analysis showed that the produced single-crystal  
7 Cu(111) almost covered the entire area without any distinct grain boundaries (Fig. 1d and  
8 Supplementary Fig. 4). The crystal orientation of the fabricated Cu(111) foil was confirmed by  
9 inverse pole figure (IPF) maps, which did not show any contrast difference in the entire area  
10 (Fig. 1e and Supplementary Figs. 5 and 6). Furthermore, X-ray diffraction (XRD) analysis  
11 verified the crystal phase and quality of the fabricated single-crystal Cu(111) foils. The XRD  
12 spectra exhibited a highly consistent sharp Cu(111) peak with a high signal-to-noise ratio (Fig. 1f  
13 and Supplementary Fig. 7).

### 14

### 15 **Synthesis of single-crystal graphene domains on $\text{Al}_2\text{O}_3(0001)$ by MPE-CVD**

16 During long-term annealing, the Cu foil gradually adhered tightly to the top surface of  
17  $\text{Al}_2\text{O}_3(0001)$ , which resulted in the formation of the ASG nanochamber in the gap between  
18 Cu(111) and  $\text{Al}_2\text{O}_3(0001)$ . The distance between Cu(111) and  $\text{Al}_2\text{O}_3(0001)$  was measured to be  
19 approximately 2.15 Å by cross-sectional high-resolution transmission electron microscopy (HR-  
20 TEM) and high-angle annular dark-field scanning transmission electron microscopy (HAADF-  
21 STEM) (Fig. 1g and Supplementary Fig. 8). The extremely small thickness of the ASG  
22 nanochamber prevented the entry of methane gas from edges of the Cu(111) foil, thereby  
23 avoiding the formation of poor-quality fractal-shaped graphene<sup>27</sup>. This was confirmed by



1 comparison in rapid CVD growth experiments (Supplementary Fig. 9). Thus, the carbon atoms  
2 could only diffuse through the Cu(111) crystal into the ASG nanochamber. Besides, atomic force  
3 microscopy (AFM) analysis revealed the ultra-flat bottom surface of the long-term-annealed  
4 Cu(111), which is significantly smoother than that of the Cu(111) top surface (Supplementary  
5 Fig. 10). The smooth surface decreased the nucleation density and increased the single-domain  
6 size of graphene, thereby preventing the formation of nanographene. Moreover, the strong van  
7 der Waals interaction and same hexagonal crystal lattice symmetry of Cu(111) and Al<sub>2</sub>O<sub>3</sub>(0001)  
8 induced a uniform superlattice potential in the ASG nanochamber, which facilitated the  
9 formation of graphene domains with the same orientation (Supplementary Fig. 11). Therefore,  
10 this ASG nanochamber was considered as an ideal platform for the synthesis of single-crystal  
11 graphene film.

12 The annealed Cu(111)/Al<sub>2</sub>O<sub>3</sub>(0001) heterostructure was placed in the MPE-CVD system  
13 for graphene synthesis that proceeded in four stages according to the main mechanism (Fig. 2a,  
14 Supplementary Fig. 12, and Supplementary Video 1): (I) carbon diffusion; (II) graphene growth;  
15 (III) plasma cleaning; and (IV) Cu removal. In stage I, the decomposed active carbon atoms  
16 partially condensed to graphene on the top surface of Cu(111) foil. Simultaneously, due to the  
17 small solubility of carbon inside the Cu(111) foil<sup>28-30</sup>, some carbon atoms dissolved into the  
18 Cu(111) crystal to form Cu-C alloys, and slowly diffused through the foil into the ASG  
19 nanochamber to act as the carbon source for the graphene growth. A dynamic secondary ion  
20 mass spectrometry (D-SIMS) depth profiling was used to study the dissolved carbon content in  
21 the Cu foils of annealing and growth processes (Supplementary Fig. 13). However, no strict time  
22 limit existed between stages I and II, which were only distinguished to highlight the difference in  
23 the main mechanism of each stage. In stage II, the diffused carbon atoms initiated nucleation and

1 formed graphene in the ASG nanochamber. Because of the uniform superlattice potential,  
2 graphene nuclei with the same crystal orientation were formed, which led to the formation of  
3 aligned graphene domains. Besides, the long-term hydrogen-annealing pretreatment almost  
4 completely removed carbon species in Cu(111) foils, which plays an essential role in the  
5 nucleation of adlayers<sup>12</sup>, leading to the growth of truly monolayer graphene. However, the top-  
6 surfaced graphene prevented carbon diffusion and decreased the catalytic efficiency during  
7 growth. Therefore, in stage III, the graphene on the top surface was removed by a hydrogen-  
8 argon plasma (Supplementary Fig. 14). During the plasma cleaning process, the graphene in the  
9 ASG nanochamber remained undamaged owing to the plasma-shielding effect of the Cu foil<sup>31</sup>.  
10 However, considering that the non-plasma-form hydrogen can diffuse into the nanochamber and  
11 etch graphene under high temperature, the system was rapidly cooled to 300 °C. During the  
12 cooling process, the Cu(111) foil shrank due to the considerable thermal expansion coefficient.  
13 This gradually weakened the interaction of the graphene with Cu(111) under the strong coupling  
14 and support of the thermally stable Al<sub>2</sub>O<sub>3</sub>(0001) substrate, preventing wrinkle formation. After  
15 stage III, the sample was quickly re-heated within seconds to the stage I of the next cycle that  
16 prevented the H<sub>2</sub> etching on as-grown graphene in the ASG nanochamber during the re-heating  
17 process. Repetition of stages I to III (multiple cycles) yielded adlayer-free ultra-flat single-crystal  
18 graphene in the ASG nanochamber. In stage IV, after the complete growth, the Cu foil was  
19 directly removed without any chemical contaminations by a designed liquid-nitrogen-assisted  
20 extreme-temperature-difference separation method (Supplementary Fig. 15).

21 After ten cycles of MPE-CVD growth, single-crystal graphene domains were directly  
22 synthesized in the ASG nanochamber (Supplementary Figs. 16 and 17). The hexagonal shape  
23 and sharp edges of aligned graphene domains indicate the high quality of the as-grown graphene

(Fig. 2b and Supplementary Fig. 18). A uniform Raman map of the  $I_D/I_G$  ratio indicates that the defects in graphene are nearly non-existent (Fig. 2c), except the weak D-band Raman signal that can be observed at the domain edge area on the Raman map of D-band intensity (Supplementary Fig. 19). The full width at half maximum (FWHM) of the 2D peak in the Raman map is approximately  $28\text{ cm}^{-1}$ , which is typical for monolayer graphene<sup>32</sup>, thus confirming that the formed graphene does not have any adlayer (Fig. 2d). These results indicate the excellent crystal structure and high quality of the directly grown graphene. Furthermore, according to typical Raman spectra, the 2D peak of the graphene directly grown on  $\text{Al}_2\text{O}_3(0001)$  was distinctly blue-shifted compared with those of transferred graphene (Fig. 2e), revealing the intense coupling and strong van der Waals interaction of graphene with the  $\text{Al}_2\text{O}_3(0001)$  substrate. The 2D peak of graphene grown on  $\text{Cu}(111)$  was more blue-shifted than that of graphene directly grown on  $\text{Al}_2\text{O}_3(0001)$  because of the stronger interaction and stress effect between graphene and  $\text{Cu}(111)$  (Fig. 2f and Supplementary Fig. 20). The statistical distributions of the 2D FWHM and  $I_{2D}/I_G$  ratio reflect the high crystal quality and absence of adlayers in the graphene grown on  $\text{Al}_2\text{O}_3(0001)$  (Fig. 2g).

### **Growth of inch-sized single-crystal graphene film on a $\text{Al}_2\text{O}_3(0001)$ wafer**

We successfully synthesized wafer-scale single-crystal monolayer graphene on the substrate of  $\text{Al}_2\text{O}_3(0001)$  by optimizing the MPE-CVD growth parameters based on the same aligned direction of crystal domains. As seen in Fig. 3a, compared to the pristine  $\text{Al}_2\text{O}_3(0001)$  wafer, the graphene/ $\text{Al}_2\text{O}_3(0001)$  exhibits a weak visible-light absorption indicated by the UV-Vis transmittance spectra at a wavelength of 350 – 800 nm. The single crystalline nature of the as-grown graphene film was verified by oxygen-plasma etching and chemically assisted

1 grain-boundary oxidization experiments (Supplementary Fig. 21). To provide direct evidence of  
2 the single-crystalline quality of the graphene directly grown on Al<sub>2</sub>O<sub>3</sub>, we applied distortion  
3 corrected low energy electron diffraction (LEED)<sup>33-35</sup>. The LEED patterns obtained  
4 (Supplementary Fig. 22) were uniform over the entire measured sample area, showing a single  
5 hexagonal structure, thereby supporting the single crystalline growth of the graphene, with the  
6 graphene adopting a commensurate registry. Naturally, such a superstructure does not result in  
7 additional LEED reflexes, albeit possible multiple scattering with spot positions  
8 indistinguishable from the substrate. Therefore, we confirmed the presence of the graphene layer  
9 on the sapphire substrate by low-temperature STM, obtaining atomically resolved images of the  
10 graphene lattice from different sample areas. The fast Fourier transforms (FFTs) of the scans  
11 reveal the uniform lattice orientation including several lower intensity frequencies not  
12 corresponding to graphene that we attribute to a Moiré contrast (Supplementary Fig. 23).

13 Further, as determined by the Raman spectral analysis, the I<sub>2D</sub>/I<sub>G</sub> ratio and the 2D peak  
14 FWHM indicate that the directly grown wafer-scale graphene film is an adlayer-free high-quality  
15 monolayer; meanwhile, the surface roughness measured from the entire wafer area represent the  
16 ultra-flat characteristic of as-grown graphene wafer (Fig. 3b). The optical micrographs and  
17 Raman maps of the 2D peak FWHM revealed the wrinkle-free smoother surface of the graphene  
18 grown directly on Al<sub>2</sub>O<sub>3</sub> compared to that of graphene grown on the upper surface of Cu and  
19 transferred to SiO<sub>2</sub>/Si, which exhibited visible wrinkles (Fig. 3c, 3d). Based on SEM images, the  
20 graphene grown directly on Al<sub>2</sub>O<sub>3</sub> has a uniform surface without any adlayer or noticeable  
21 wrinkles (Fig. 3e), whereas the SiO<sub>2</sub>/Si-based transferred graphene exhibits a distinct wrinkle  
22 network (Fig. 3f). The graphene surfaces were analyzed by AFM, which revealed a smooth  
23 surface for the graphene grown directly on Al<sub>2</sub>O<sub>3</sub> and rough surface with distinct wrinkles for the

1 transferred graphene (Fig. 3g and Supplementary Fig. 24). HR-TEM images show the clean  
2 surface and perfect honeycomb structure of graphene grown directly on Al<sub>2</sub>O<sub>3</sub> (Fig. 3h).  
3 Moreover, the crystal lattice orientations determined from the selected area electron diffraction  
4 (SAED) patterns obtained from various locations across the 3 mm diameter sample indicate the  
5 highly consistent single crystalline structure of the as-grown graphene.

### 6 7 **Physical mechanisms and DFT simulation**

8 The underlying physical mechanisms of the experimental observations were investigated  
9 by simulations based on density functional theory (DFT). Nine models were built using Cu(110),  
10 Cu(100), Cu(111), Al<sub>2</sub>O<sub>3</sub>(11-20), Al<sub>2</sub>O<sub>3</sub>(10-10), and Al<sub>2</sub>O<sub>3</sub>(0001) surfaces, which were analyzed  
11 in terms of crystal symmetry and lattice mismatch (Supplementary Fig. 25). The combination of  
12 Cu(111) and Al<sub>2</sub>O<sub>3</sub>(0001) exhibited a hexagonal symmetry and the best lattice consistency with a  
13 minimal lattice mismatch of 6.5%. The stacking energies per Cu atom were 0.98, 1.33, and 2.09  
14 eV for Cu(110), Cu(100), and Cu(111), respectively, indicating that Cu(111) is energetically  
15 favorable (Fig. 4a, 4b). The interaction between the Cu foil and Al<sub>2</sub>O<sub>3</sub> substrate was further  
16 investigated by simulating both O-terminated and Al-terminated Al<sub>2</sub>O<sub>3</sub>(0001) (Supplementary  
17 Fig. 26 and Supplementary Table 1). The higher energy states of Cu(110) and Cu(100) caused by  
18 the larger lattice mismatch resulted in gradual conversion to Cu(111) when the temperature  
19 approached the melting temperature.

20 During the MPE-CVD process, the active carbon atoms dissolved into the Cu foil to form  
21 a Cu–C alloy at high temperature and gradually diffused through the foil to the  
22 Cu(111)/Al<sub>2</sub>O<sub>3</sub>(0001) interface<sup>36</sup> (Fig. 4c). This carbon diffusion process was investigated by  
23 finite element simulations based on Fick's laws and convection-diffusion equations<sup>37,38</sup>

1 (Supplementary Fig. 27). Guided by the simulation results, the experimental MPE-CVD growth  
2 process was adjusted with a specially designed temperature-variation carbon-dissolution strategy  
3 to ensure the continuous diffusion of carbon atoms. The carbon binding energies of graphene on  
4 Cu(111), on Al<sub>2</sub>O<sub>3</sub>(0001), and at the Cu(111)/Al<sub>2</sub>O<sub>3</sub>(0001) interface, determined by simulations,  
5 were 0.204, 0.200, and 0.304 eV, respectively, indicating the feasibility of graphene growth at  
6 the interface (Fig. 4d). Furthermore, the binding energies of graphene on the O-terminated and  
7 Al-terminated Al<sub>2</sub>O<sub>3</sub>(0001) were 0.304 and 0.081 eV per carbon atom, respectively  
8 (Supplementary Fig. 28 and Supplementary Table 2). Because of the crystal symmetry and small  
9 lattice mismatch between Cu(111) and Al<sub>2</sub>O<sub>3</sub>(0001), a Moiré superlattice was formed when the  
10 two materials were stacked with a twist angle (Supplementary Fig. 29), which rightfully has the  
11 matching lattice period with graphene (Fig. 4e). Under these conditions, the graphene domains  
12 grew with the same crystal orientation and subsequently merged to form a single-crystalline  
13 graphene film between Cu(111) and Al<sub>2</sub>O<sub>3</sub>(0001).

## 14 15 **Potential applications of ultra-high-quality graphene**

16 The absence of an ideal synthesis method that can overcome the drawbacks of  
17 conventional CVD growth and avoid problems associated with transfer processes remains the  
18 bottleneck of the practical application of graphene in advanced carbon-based nanodevice fields.  
19 In this work, we directly grew high-quality graphene at the interface of a metal-insulator by  
20 utilizing the specifically designed ASG nanochamber formed between Cu(111) and Al<sub>2</sub>O<sub>3</sub>(0001)  
21 through MPE-CVD growth. Owing to the pre-removal of carbon species, Cu(111)–Al<sub>2</sub>O<sub>3</sub>(0001)  
22 interface growth, and superlattice potential confinement, an adlayer-free ultra-flat single-crystal  
23 monolayer graphene was directly achieved on an insulating substrate. This direct growth

1 technology for graphene enables the exploration of next-generation carbon-based high-  
2 performance integrated electronics and facilitates the fulfillment of the potential of graphene in  
3 various fields. Most importantly, this work provides a new approach for the design and  
4 development of ideal epitaxial templates to grow wafer-scale single-crystal bilayer graphene or  
5 other single-crystal 2D materials (Supplementary Figs. 30 and 31), and form Moiré  
6 heterostructures thereby accelerating the research of magic angle materials on macroscale  
7 samples for fundamental research in the field of physics.

### 9 **Online content**

10 Any methods, additional references, Nature Research reporting summaries, source data, extended  
11 data, supplementary information, acknowledgements, peer review information; details of author  
12 contributions and competing interests; and statements of data and code availability are available  
13 at <https://doi.org/xxxx>.

## References

- 1 Geim, A. K. Graphene: status and prospects. *Science* **324**, 1530-1534 (2009).
- 2 Novoselov, K. S. *et al.* A roadmap for graphene. *Nature* **490**, 192-200 (2012).
- 3 Akinwande, D. *et al.* Graphene and two-dimensional materials for silicon technology. *Nature* **573**, 507-518 (2019).
- 4 Cao, Y. *et al.* Correlated insulator behaviour at half-filling in magic-angle graphene superlattices. *Nature* **556**, 80-84 (2018).
- 5 Cao, Y. *et al.* Unconventional superconductivity in magic-angle graphene superlattices. *Nature* **556**, 43-50 (2018).
- 6 Li, X. *et al.* Large-area synthesis of high-quality and uniform graphene films on copper foils. *Science* **324**, 1312-1314 (2009).
- 7 Vlassioux, I. V. *et al.* Evolutionary selection growth of two-dimensional materials on polycrystalline substrates. *Nat Mater* **17**, 318-322 (2018).
- 8 Kim, Y. *et al.* Synthesis of high quality graphene on capped (1 1 1) Cu thin films obtained by high temperature secondary grain growth on c-plane sapphire substrates. *2D Materials* **5**, 035008 (2018).
- 9 Zhang, X. *et al.* Epitaxial growth of 6 in. single - crystalline graphene on a Cu/Ni (111) film at 750° C via chemical vapor deposition. *Small* **15**, 1805395 (2019).
- 10 Huang, M. *et al.* Highly oriented monolayer graphene grown on a Cu/Ni (111) alloy foil. *ACS nano* **12**, 6117-6127 (2018).
- 11 Wu, T. *et al.* Fast growth of inch-sized single-crystalline graphene from a controlled single nucleus on Cu-Ni alloys. *Nature Mater.* **15**, 43-47 (2016).
- 12 Luo, D. *et al.* Adlayer-Free Large-Area Single Crystal Graphene Grown on a Cu(111) Foil. *Adv. Mater.* **1903615**, 1-13 (2019).
- 13 Yuan, G. *et al.* Proton-assisted growth of ultra-flat graphene films. *Nature* **577**, 204-208 (2020).
- 14 Pirkle, A. *et al.* The effect of chemical residues on the physical and electrical properties of chemical vapor deposited graphene transferred to SiO<sub>2</sub>. *Appl. Phys. Lett.* **99**, 122108 (2011).
- 15 Chen, J. *et al.* Oxygen-aided synthesis of polycrystalline graphene on silicon dioxide substrates. *J. Am. Chem. Soc.* **133**, 17548-17551 (2011).
- 16 Chen, X. D. *et al.* Fast Growth and Broad Applications of 25-Inch Uniform Graphene Glass. *Adv. Mater.* **29**, 1603428 (2017).
- 17 Pan, G. H. *et al.* Transfer-free growth of graphene on SiO<sub>2</sub> insulator substrate from sputtered carbon and nickel films. *Carbon* **65**, 349-358 (2013).
- 18 Su, C. Y. *et al.* Direct formation of wafer scale graphene thin layers on insulating substrates by chemical vapor deposition. *Nano Lett.* **11**, 3612-3616 (2011).
- 19 Kim, H. *et al.* Copper-vapor-assisted chemical vapor deposition for high-quality and metal-free single-layer graphene on amorphous SiO<sub>2</sub> substrate. *ACS nano* **7**, 6575-6582 (2013).
- 20 Mishra, N. *et al.* Wafer - scale synthesis of graphene on sapphire: toward fab - compatible graphene. *Small* **15**, 1904906 (2019).
- 21 Wu, M. *et al.* Seeded growth of large single-crystal copper foils with high-index facets. *Nature* **581**, 406-410 (2020).
- 22 Meiners, T., Frolov, T., Rudd, R. E., Dehm, G. & Liebscher, C. H. Observations of grain-boundary phase transformations in an elemental metal. *Nature* **579**, 375-378 (2020).



- 1 23 Li, B. W. *et al.* Orientation-Dependent Strain Relaxation and Chemical Functionalization  
2 of Graphene on a Cu(111) Foil. *Adv. Mater.* **30**, 1706504 (2018).
- 3 24 Chen, T. A. *et al.* Wafer-scale single-crystal hexagonal boron nitride monolayers on Cu  
4 (111). *Nature* **579**, 219-223 (2020).
- 5 25 Jin, S. *et al.* Colossal grain growth yields single-crystal metal foils by contact-free  
6 annealing. *Science* **362**, 1021-1025 (2018).
- 7 26 Constable, F. H. The cause of the colours shown during the oxidation of metallic copper.  
8 *Proc. R. Soc. London, Ser. A* **115**, 570-588 (1927).
- 9 27 Li, J. *et al.* Fractal-Theory-Based Control of the Shape and Quality of CVD-Grown 2D  
10 Materials. *Adv. Mater.* **1902431**, 1-7 (2019).
- 11 28 Wu, T. *et al.* Fast growth of inch-sized single-crystalline graphene from a controlled  
12 single nucleus on Cu–Ni alloys. *Nature Mater.* **15**, 43-47 (2016).
- 13 29 Zhao, Z. *et al.* Study on the diffusion mechanism of graphene grown on copper pockets.  
14 *Small* **11**, 1418-1422 (2015).
- 15 30 Fuks, D. *et al.* Carbon in copper and silver: Diffusion and mechanical properties. *Journal*  
16 *of Molecular Structure: THEOCHEM* **539**, 199-214 (2001).
- 17 31 Morgan, W. L., Whitten, B. L. & Bardsley, J. N. Plasma shielding effects on ionic  
18 recombination. *Phys. Rev. Lett.* **45**, 2021-2024 (1980).
- 19 32 Ferrari, A. C. *et al.* Raman spectrum of graphene and graphene layers. *Phys. Rev. Lett.*  
20 **97**, 187401 (2006).
- 21 33 Sojka, F., Meissner, M., Zwick, C., Forker, R. & Fritz, T. Determination and correction  
22 of distortions and systematic errors in low-energy electron diffraction. *Rev. Sci. Instrum.*  
23 **84**, 015111 (2013).
- 24 34 Sojka, F. *et al.* To tilt or not to tilt: Correction of the distortion caused by inclined sample  
25 surfaces in low-energy electron diffraction. *Ultramicroscopy* **133**, 35-40 (2013).
- 26 35 Schaal, M. *et al.* Hybridization vs decoupling: influence of an h-BN interlayer on the  
27 physical properties of a lander-type molecule on Ni (111). *Beilstein journal of*  
28 *nanotechnology* **11**, 1168-1177 (2020).
- 29 36 Berner, A. *et al.* Microstructure of Cu-C interface in Cu-based metal matrix composite.  
30 *Sens. Actuator A Phys.* **74**, 86-90 (1999).
- 31 37 Kurganov, A. & Tadmor, E. New high-resolution central schemes for nonlinear  
32 conservation laws and convection-diffusion equations. *J. Comput. Phys.* **160**, 241-282  
33 (2000).
- 34 38 Paradisi, P., Cesari, R., Mainardi, F. & Tampieri, F. The fractional Fick's law for non-  
35 local transport processes. *Physica A Stat. Mech. Appl.* **293**, 130-142 (2001).

36  
37 **Publisher's note** Springer Nature remains neutral with regard to jurisdictional claims in  
38 published maps and institutional affiliations.

39 © The Author(s), under exclusive licence to Springer Nature Limited 2020

## 1       **Methods**

2       **Preparation of single crystal Cu foils on Al<sub>2</sub>O<sub>3</sub>(0001).** The as-received polycrystalline Cu foil  
3 (25 μm thick, 99.9% purity from Nilaco Co.) was electrochemically polished in the polishing  
4 solution (Contents: H<sub>2</sub>PO<sub>4</sub>, ethanol, isopropyl alcohol, and urea), and cleaned with ethanol. The  
5 as-received Al<sub>2</sub>O<sub>3</sub>(0001) substrate (10 mm × 10 mm or 2-inch, c-plane, and double-sided  
6 polished from 11-D Tech) was cleaned sequentially with acetone, isopropanol (IPA), and  
7 deionized (DI) water for 5 min in each solvent and deeply cleaned with an H<sub>2</sub>SO<sub>4</sub>: H<sub>3</sub>PO<sub>4</sub>  
8 mixture (3:1) at 300 °C for 25 min. It was cleaned again with DI water and then finally by  
9 oxygen plasma. Next, the polished Cu foil was flattened by a regular laminator using a protection  
10 of PET film on both sides. Then, the Cu foil was placed on the surface of the cleaned  
11 Al<sub>2</sub>O<sub>3</sub>(0001) substrate. The Cu foil got attached to the surface spontaneously due to the adhesion  
12 effect. The Cu/Al<sub>2</sub>O<sub>3</sub>(0001) substrate was then placed in a quartz boat and inserted into a 3-inch  
13 diameter quartz tube of the CVD system. The substrate was heated to 1350 K in an atmosphere  
14 of H<sub>2</sub> (99.999%) and Ar (99.999%) with flow rates of 50 and 50 sccm, respectively, at a pressure  
15 of 750 torr for 24 h – 30 h. The total annealing time is slightly different and depends on the  
16 initial Cu foil size. During this period, the polycrystalline Cu foil gradually transforms into single  
17 crystal Cu(111). Then, the system was cooled down from 1350 K to 373 K with average cooling  
18 rates of 80 K/min and from 373 K to room temperature at 10 K/min. After annealing, the  
19 Cu(111) foil adhered firmly to the Al<sub>2</sub>O<sub>3</sub>(0001) substrate to form the Cu(111)/Al<sub>2</sub>O<sub>3</sub>(0001)  
20 heterostructure.

21       **Growth of graphene via MPE-CVD.** Graphene was synthesized in the ASG nanochamber  
22 between the Cu(111)/Al<sub>2</sub>O<sub>3</sub>(0001) heterostructure by the MPE-CVD method using mixtures of  
23 CH<sub>4</sub>, H<sub>2</sub>, and Ar. First, the long-term-annealed Cu(111)/Al<sub>2</sub>O<sub>3</sub>(0001) heterostructure was placed  
24 in the MPE-CVD system. Next, the system was heated to 1075 °C and the gases H<sub>2</sub> and Ar were  
25 allowed to flow at a rate of 50 and 350 sccm, respectively, at a pressure of 3 torr. Then, CH<sub>4</sub>  
26 (99.999 %) with a flow rate of 10 sccm was purged into the tube. During this period, the carbon  
27 atoms dissolved into Cu and some graphene domains could start nucleation and growth on the  
28 top surface and also inside the ASG nanochamber. After 60 min, the system was cooled to 1050  
29 °C for 30 min, to reach a conducive temperature for higher-quality graphene growth. Then,  
30 diluted CH<sub>4</sub> gas (0.1 % diluted in Ar) with a flow rate of 10 sccm was purged into the system to  
31 maintain a high H<sub>2</sub>/CH<sub>4</sub> ratio and provide continuous carbon feeding during this period, with 10  
32 sccm H<sub>2</sub> and 50 sccm Ar gas flow at 0.5 torr for 30 min. Subsequently, the system was slowly  
33 cooled down to 300 °C in 20 min to avoid quick shrinking of the Cu foil. Then, the CH<sub>4</sub> gas flow  
34 was stopped and the flow rate of H<sub>2</sub> was increased to 30 sccm; the plasma unit (200 W) was  
35 moved to the sample position and switched on for 3 min to clean the graphene on the Cu upper  
36 surface. Meanwhile, the tube furnace was heated to 1075 °C at the empty position (left side of  
37 the sample position). After plasma-etching process and waiting for the temperature of furnace to  
38 stabilize at 1075 °C, the H<sub>2</sub> gas flow was stopped and the furnace was quickly moved back to the  
39 sample position. The sample was reheated to 1075 °C within 5 seconds, which can prevent the  
40 etching of graphene by H<sub>2</sub> during the heating process. Then, the above processes were performed  
41 in cycle several times to obtain the final samples with single-crystal graphene in the ASG  
42 nanochamber.

1 **Growth of single-crystal monolayer h-BN on Cu(111)/Al<sub>2</sub>O<sub>3</sub>(0001).** A 300-nm Cu film was  
2 deposited on an Al<sub>2</sub>O<sub>3</sub>(0001) substrate and then annealed for 1h to form the Cu(111) film. The  
3 Cu(111)/Al<sub>2</sub>O<sub>3</sub>(0001) was then placed in a 3-inch CVD system. Borane-ammonia (97%, from  
4 Aldrich) was used as the precursor and loaded into a second tube. The system was heated to 1050  
5 °C with 20-sccm H<sub>2</sub>. After a 20-min annealing process, the precursor was heated to 90 °C with 5-  
6 sccm Ar as the carrier gas. Next, the precursor was introduced into the main tube for 30 min to  
7 grow h-BN on the Cu(111)/Al<sub>2</sub>O<sub>3</sub>(0001) substrates. After h-BN film growth, the furnace was  
8 programmed to fast cool to 100 °C in 10 min, and then cooled down to room temperature in 30  
9 min.

10 **Growth of aligned h-BN domains on direct-grown graphene.** Aligned h-BN domains were  
11 grown by a similar method to the growth of single-crystal monolayer h-BN on  
12 Cu(111)/Al<sub>2</sub>O<sub>3</sub>(0001); the difference was to replace the Cu foil with the as-grown single-crystal  
13 graphene/Al<sub>2</sub>O<sub>3</sub>(0001). The Cu foil was placed on the top of the graphene to work as the catalyst.

14 **Growth of aligned MoS<sub>2</sub> domains on direct-grown graphene.** As-grown single-crystal  
15 graphene/Al<sub>2</sub>O<sub>3</sub>(0001) was used as a growth substrate for the synthesis of MoS<sub>2</sub> film. MoO<sub>3</sub>  
16 powder (99.5%, Sigma-Aldrich) and sulfur powder (99%, Sigma-Aldrich) were supplied as the  
17 precursor for MoS<sub>2</sub> growth. The MoO<sub>3</sub> powder was placed in a boat, and the single-crystal  
18 graphene/Al<sub>2</sub>O<sub>3</sub>(0001) substrate was faced down and mounted on the top of the boat. A separate  
19 boat with sulfur powder was placed next to the MoO<sub>3</sub> powder. Then, the reaction chamber was  
20 heated to the growing temperature (600–800 °C) at a rate of 50 °C min<sup>-1</sup>. The MoS<sub>2</sub> domains  
21 were grown at 800 °C for 15 min using a carrier gas flow rate of 10-sccm Ar. After growth, the  
22 heating furnace was quickly cooled down to room temperature.

23 **Transfer of conventionally grown graphene onto arbitrary substrates.** The conventionally  
24 grown graphene was spin-coated for 1 min by poly(methyl methacrylate) (950 PMMA C4) and  
25 then was heated at 120 °C for 20 min. Next, the Cu foil was etched using a 0.03g/ml (NH<sub>4</sub>)<sub>2</sub>S<sub>2</sub>O<sub>8</sub>  
26 solution. After that, the arbitrary substrate was used to hold the PMMA/graphene and dried in air  
27 for 1 h. Then, the samples were placed in an oven and baked at 120 °C for 30 min. Finally,  
28 acetone was used to remove the PMMA.

29 **Characterization methods.** Raman spectra and mapping of graphene, h-BN, and MoS<sub>2</sub> were  
30 obtained by confocal Raman spectroscopy (Alpha 300R, WITec) with 488 nm and 532 nm solid-  
31 state laser; 488 nm and 532 nm laser were used for the characterization of 2D materials on the  
32 Cu substrate and the insulating substrates, respectively. UV–Vis transmittance spectra were  
33 measured using a UV–Vis spectrophotometer (Lambda 950, PerkinElmer). Scanning electron  
34 microscopy (SEM, Merlin, Zeiss) was used to observe the morphology of graphene. The electron  
35 backscatter diffraction accessory (EBSD, Oxford Instruments) in the SEM (Quanta 600, FEI)  
36 was used to characterize the crystal phase of the Cu foil. The surface morphologies of Cu and  
37 graphene were characterized by atomic force microscopy (AFM, Dimension Icon, Bruker). X-ray  
38 diffraction (XRD, D2 PHASER, Bruker) patterns were obtained from the fabricated Cu foil. The  
39 cross-sectional TEM specimens were prepared using the focused ion beam (FIB, Helios 400S,  
40 FEI) technique. To protect the sample from ion beam damages, it was passivated using electron  
41 beam assisted Pt deposition (300 nm) before exposing it to the ion beam. HR-TEM imaging,

1 HAADF-STEM imaging, and EDS mapping were performed on a transmission electron  
2 microscope (TEM, Titan Themis Z, FEI) equipped with a high-brightness electron gun (x-FEG),  
3 an electron beam monochromator, and a double Cs corrector operated at 300 kV. UHV-STM  
4 measurements were carried out in a low-temperature STM (SPECS Surface Nano Analysis  
5 GmbH), operated at 4.5 K and a base pressure of  $1.0 \times 10^{-10}$  Torr, using a tungsten tip. Low  
6 energy electron diffraction (LEED) with beam diameter of approximately 1 mm was performed  
7 in an ultrahigh vacuum chamber with a base pressure of  $1.0 \times 10^{-10}$  Torr. In order to prevent  
8 charging of the insulating substrate, a double multi-channel plate (MCP) LEED (MCP2-LEED,  
9 OCI Vacuum Microengineering) was used, and the graphene layer was contacted from the top by  
10 use of a molybdenum mask sparing a circular measurement area. Further, we applied distortion  
11 correction to the LEED images, as described in the literature<sup>33,34</sup>, by applying the software  
12 LEEDLab and LEEDCal<sup>35</sup>. Depth profiling experiments were performed on a dynamic  
13 secondary ion mass spectrometer (D-SIMS, Hiden Analytical, UK) operated under ultra-high  
14 vacuum conditions, typically  $10^{-9}$  torr. A continuous  $\text{Ar}^+$  beam of 4 keV energy was employed to  
15 sputter the surface while the selected ions were sequentially collected using a MAXIM  
16 spectrometer equipped with a quadrupole analyzer.

17 **DFT simulations.** All simulations were carried out by the Vienna *ab initio* Simulation Package  
18 (VASP) using the projector augmented wave method and Perdew-Burke-Ernzerhof form of the  
19 generalized gradient approximation for the electron exchange-correlation potential<sup>39,40</sup>. The  
20 Grimme method was used for van der Waals correction<sup>41</sup>. A cutoff energy of 500 eV was chosen  
21 for the plane-wave expansion. The force criterion for the structural relaxation was set to 0.001  
22 eV/Å, and a  $7 \times 7 \times 1$  *k*-mesh was used. To minimize the lattice mismatch between the  
23 components,  $2 \times 2 \times 1$  supercells of Cu(111) and graphene were combined with a unit cell of  
24  $\text{Al}_2\text{O}_3(0001)$ . A 14.67 Å thick nine-layer slab of Cu(111) was used, with five layers fixed to the  
25 bulk structure and four layers free to relax. An 11.15 Å thick O-terminated or 10.15 Å thick Al-  
26 terminated five-layer slab of  $\text{Al}_2\text{O}_3(0001)$  was added, with three layers fixed to the bulk structure  
27 and two layers free to relax. The slab model was completed with a 20 Å thick vacuum layer.

#### 28 **Data availability**

29 The data that support the findings of this study are available from the corresponding author upon  
30 reasonable request.

#### 31 **References**

- 32 39 Perdew, J. P., Burke, K. & Ernzerhof, M. Phys rev lett 77: 3865. *Phys. Rev. Lett.* **78**,  
33 1396 (1996).  
34 40 Kresse, G. Comput. matter sci. 6, 15 (1996);(d) kresse, g., and furthmuller. *Phys. Rev. B*  
35 **54**, 11,169 (1996).  
36 41 Grimme, S., Antony, J., Ehrlich, S. & Krieg, H. A consistent and accurate ab initio  
37 parametrization of density functional dispersion correction (DFT-D) for the 94 elements  
38 H-Pu. *J. Chem. Phys* **132**, 154104 (2010).  
39

#### 40 **Acknowledgments**

41 We thank R. S. Ruoff for comments on manuscript preparation. We thank Y. Gao and F. Laquai  
42 for help with UV-Vis spectrum measurement, and N. Wehbe for help with D-SIMS  
43 measurement. This work was supported by King Abdullah University of Science and

1 Technology (KAUST), under award numbers: OSR-2018-CRG7-3717 and OSR-2016-CRG5-  
2 2996.

### 3 **Author contributions**

4 J.L. and B.T. conceived the experiments. X.Z. supervised the project. J.L. and H.D. performed  
5 the annealing of the Cu foils and their characterizations. J.L., M.C. and H.D. performed the  
6 graphene growth and transfer experiments. J.L., H.D. and B.T. performed the Raman, SEM,  
7 AFM, and XRD characterizations. J.Z. performed the TEM characterization for 2D materials.  
8 C.C., Y.H. and B.T. performed the FIB, HR-TEM, HAADF-STEM, and EDS characterizations  
9 for the cross-section. J.D. and T.F. performed the LEED and STM characterizations. A.S., A.R.  
10 and U.S. performed the DFT simulations. M.C., U.S., T.F. and X.Z. provided comments on the  
11 manuscript. J.L. and B.T. wrote the manuscript. All coauthors revised and commented on the  
12 manuscript.

### 13 **Competing interests**

14 The authors declare no competing interests.

### 15 **Additional information**

16 **Supplementary information** is available for this paper at <https://doi.org/xxx>.

17 **Correspondence and requests for materials** should be addressed to B.T. or X.Z.

18 **Reprints and permissions information** is available at <http://www.nature.com/reprints>.

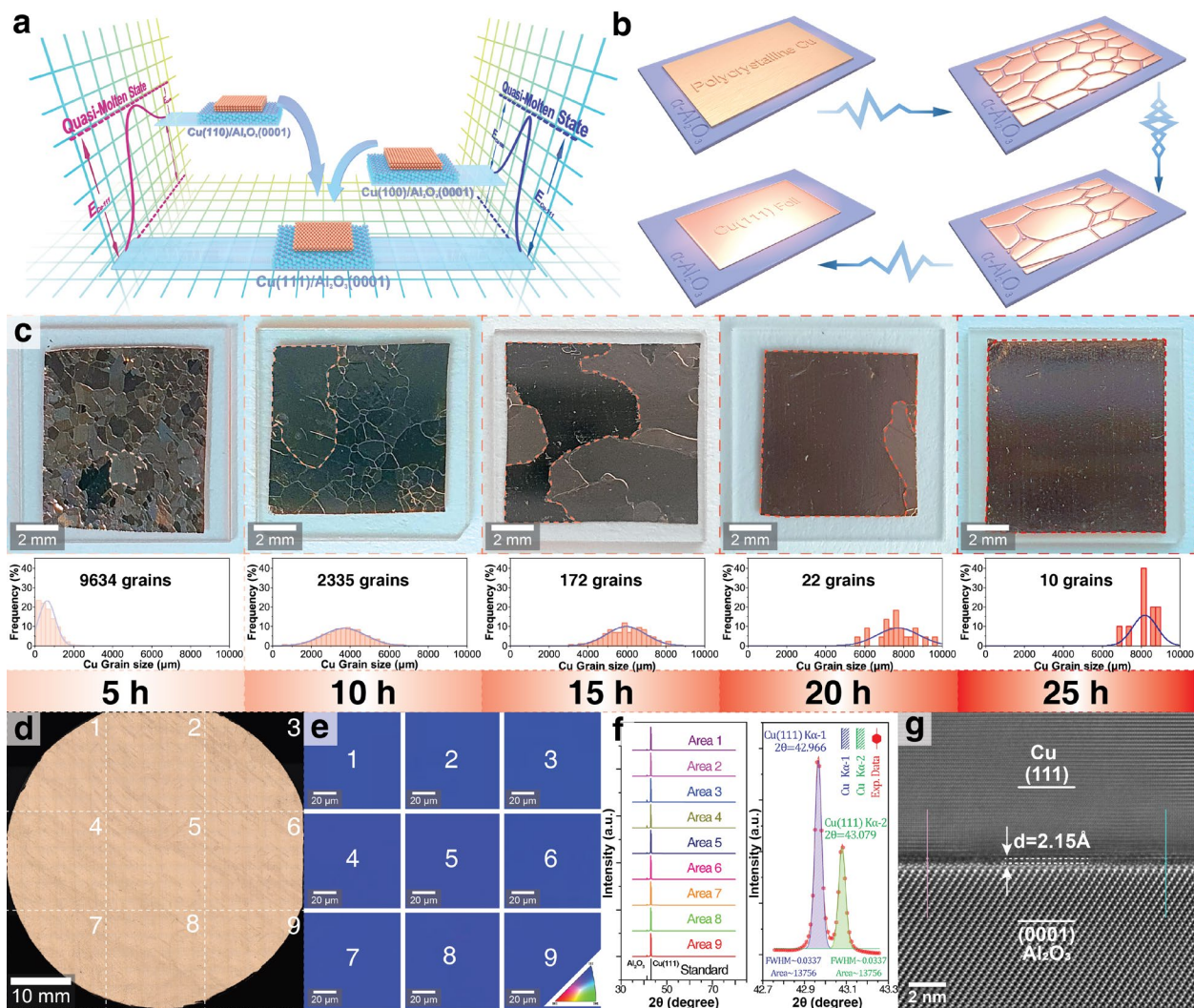
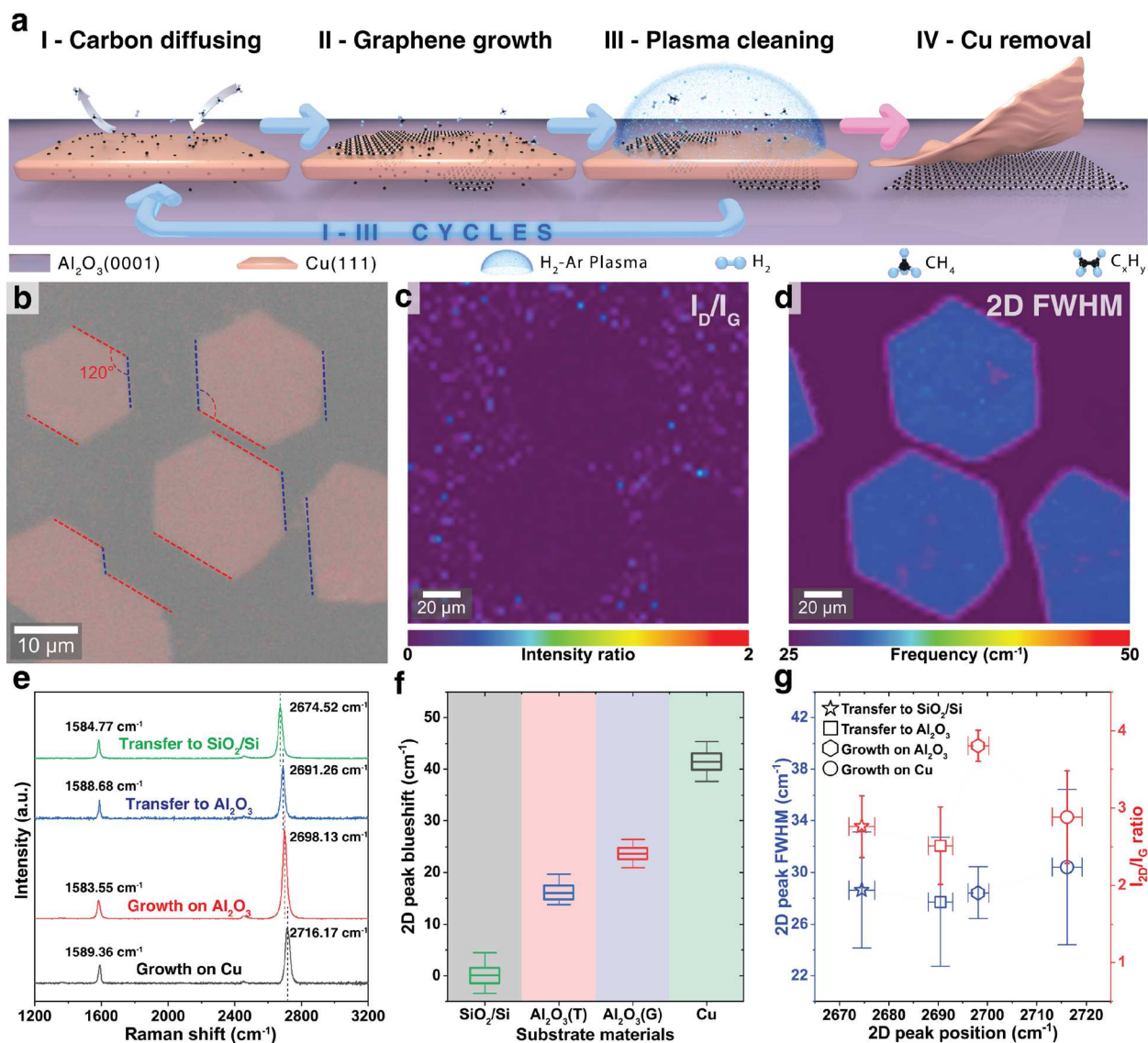


**Fig. 1 | Wafer-scale single-crystal Cu(111) foil formed on  $\text{Al}_2\text{O}_3(0001)$ .** **a**, Energy diagram of  
**2** Cu(110), Cu(100), and Cu(111) crystals on an  $\text{Al}_2\text{O}_3(0001)$  surface. **b**, Schematic of the  
**3** transformation process from a commercial polycrystalline Cu foil into a single-crystal Cu(111)  
**4** foil on  $\text{Al}_2\text{O}_3(0001)$ . **c**, Photograph of Cu foil ( $10 \times 10 \text{ mm}^2$ ) annealed for various periods (5–25  
**5** h). The largest Cu grain of each sample is indicated by the dashed contour. Corresponding Cu  
**6** grain size distributions obtained by measuring 10 samples for each annealing time are also  
**7** shown. **d**, Optical micrograph of the fabricated 2-inch single-crystal Cu(111) foil. The area is  
**8** divided into nine parts for further characterization. **e**, EBSD IPF maps of the nine areas in (d). **f**,  
**9** XRD spectra of the marked areas in (d). A distinct peak-split of the Cu(111)  $\text{K}\alpha$ -1 and  $\text{K}\alpha$ -2  
**10** peaks is observed in the enlarged image (right) due to the ultra-high crystallinity of the fabricated  
**11** Cu(111) foil. **g**, Cross-sectional HR-TEM image of the Cu(111)/ $\text{Al}_2\text{O}_3(0001)$  interface. The  
**12** width of the boundary formed between Cu and  $\text{Al}_2\text{O}_3$  was determined from the intensity profiles  
**13** along the magenta and blue lines (see Supplementary Fig. 8 for detailed analysis).



1 **Fig. 2 | Growth of single-crystal graphene in ASG nanochamber.** **a**, Schematic of the  
 2 graphene formation process in the ASG nanochamber during MPE-CVD. **b**, Optical micrograph  
 3 of graphene domains directly grown on Al<sub>2</sub>O<sub>3</sub>(0001). The aligned orientation of individual  
 4 hexagonal domains is indicated by dashed lines. **c**, Raman map of I<sub>D</sub>/I<sub>G</sub> ratios of graphene  
 5 crystals in the region shown in (b). **d**, 2D FWHM Raman map of graphene crystals in the region  
 6 shown in (b). **e**, Representative Raman spectra of graphene grown directly on Al<sub>2</sub>O<sub>3</sub> (red),  
 7 graphene grown on the upper surface of Cu foil without transfer after removing the Cu  
 8 fluorescence (black), graphene grown on upper surface of Cu foil and then transferred to  
 9 Al<sub>2</sub>O<sub>3</sub>(0001) (blue), and 300 nm SiO<sub>2</sub>/Si wafer (green). **f**, 2D peak blueshift of four types of  
 10 graphene mentioned in (e). The 2D peak position of the SiO<sub>2</sub>/Si-based transferred graphene is  
 11 considered as the reference. **g**, 2D peak FWHM and I<sub>2D</sub>/I<sub>G</sub> ratio of 20 samples of each type of  
 12 graphene mentioned in (e). A Raman laser with 532 nm wavelength is used for Al<sub>2</sub>O<sub>3</sub> and  
 13 SiO<sub>2</sub>/Si substrate, and 488 nm wavelength is used for Cu substrate.

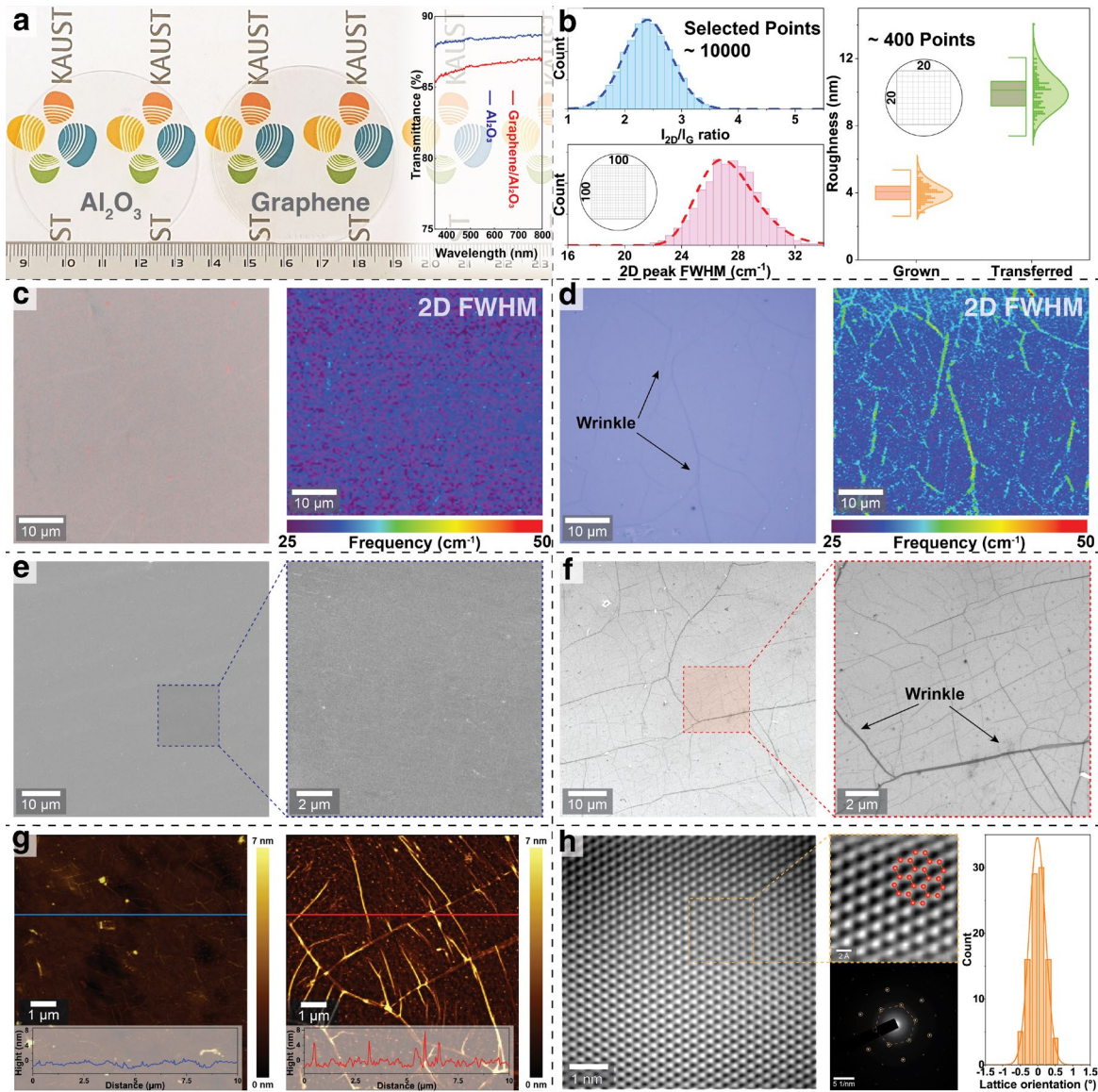
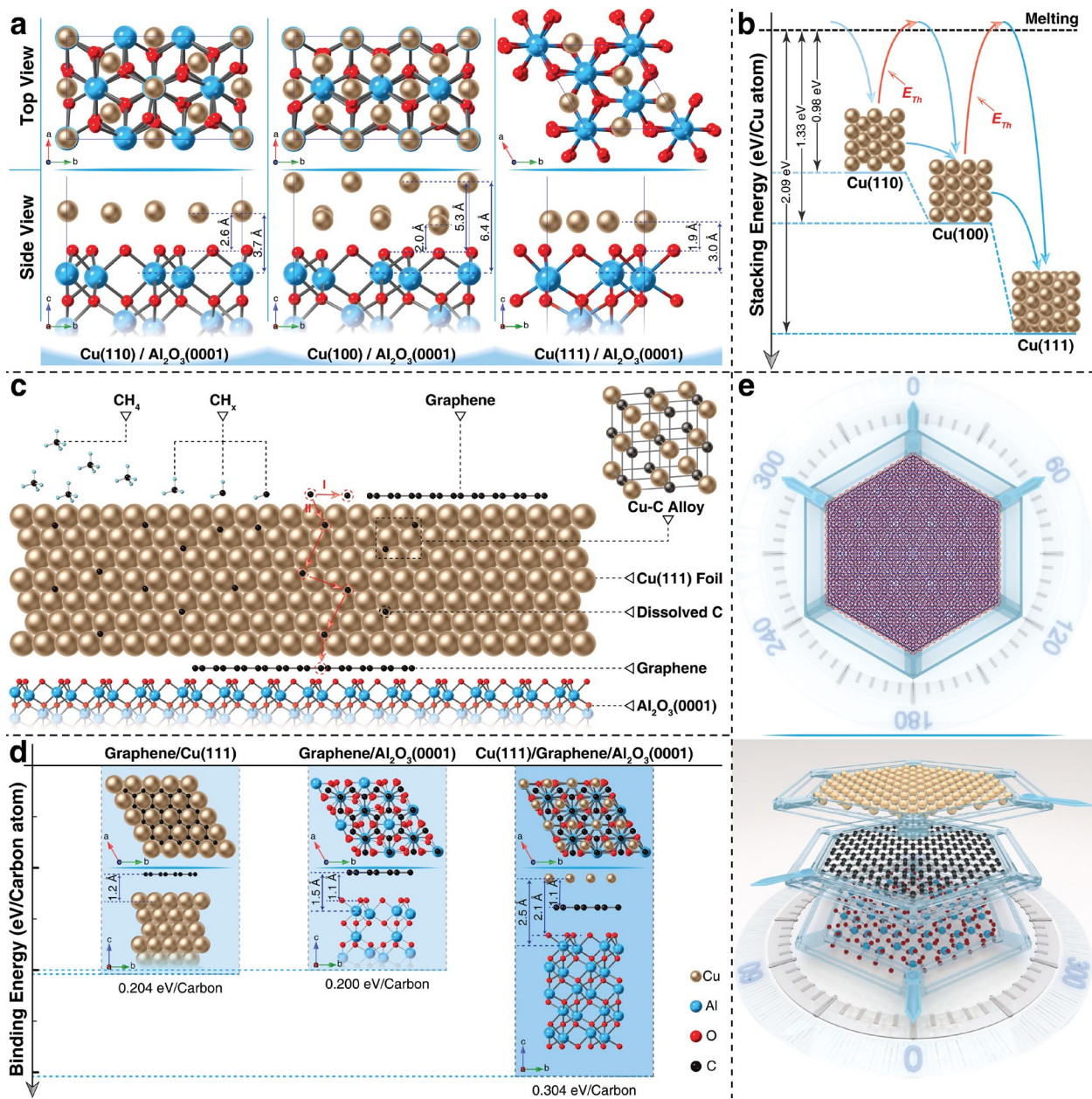


**Fig. 3 | Synthesis of wafer-scale single-crystal graphene film on  $\text{Al}_2\text{O}_3(0001)$ .** **a**, Photograph and UV-Vis transmittance spectra in the wavelength range of 350 – 800 nm of the  $\text{Al}_2\text{O}_3(0001)$  wafer without graphene (left) and with as-grown graphene (right). **b**, Raman signals of  $I_{2D}/I_G$  intensity ratio (cyan) and 2D peak FWHM (magenta) collected from 10,000 points ( $100 \times 100$  array) with 300  $\mu\text{m}$  step length (left); surface roughness of graphene grown directly on  $\text{Al}_2\text{O}_3$  and graphene grown on the upper surface of Cu and transferred to  $\text{Al}_2\text{O}_3$  measured by AFM with 400 pixels ( $20 \times 20$  array) (right). **c**, Optical image (left) and Raman map of 2D peak FWHM (right) of graphene grown directly on  $\text{Al}_2\text{O}_3(0001)$ . **d**, Optical image (left) and Raman map of 2D peak FWHM (right) of graphene on Cu and then transferred on  $\text{SiO}_2/\text{Si}$  substrate. The wrinkles are indicated by the arrows. **e**, SEM image of graphene grown directly on  $\text{Al}_2\text{O}_3(0001)$ . **f**, SEM image of graphene grown on the upper surface of Cu and transferred to  $\text{SiO}_2/\text{Si}$ . **g**, AFM image of graphene grown directly on  $\text{Al}_2\text{O}_3(0001)$  (left) and transferred  $\text{SiO}_2/\text{Si}$ -based graphene (right). The height profiles along the marked line are plotted in the bottom inset. **h**, High-resolution TEM image of directly grown graphene. Distribution of graphene orientation angles measured from SAED patterns at different positions over 3 mm diameter TEM grid.





1 **Fig. 4 | DFT simulations and carbon-diffusion model.** **a**, Atomic structures of Cu on  
2 Al<sub>2</sub>O<sub>3</sub>(0001) after relaxation. Top view from the <0001> direction and side view from the <11-  
3 20> direction. Cu, Al, and O atoms are shown in gold, blue, and red, respectively. **b**, Stacking  
4 energies of Cu(100), Cu(110), and Cu(111) on Al<sub>2</sub>O<sub>3</sub>(0001). **c**, Schematic of carbon diffusion  
5 through the Cu(111) foil and formation of a Cu-C alloy. **d**, Atomic structures and carbon binding  
6 energies for graphene on Cu(111), graphene on Al<sub>2</sub>O<sub>3</sub>(0001), and graphene between Cu(111) and  
7 Al<sub>2</sub>O<sub>3</sub>(0001). **e**, Schematic of the sandwich structure formed by Cu(111), graphene, and  
8 Al<sub>2</sub>O<sub>3</sub>(0001), showing a Moiré superlattice pattern with 60° twist angle between the layers.

## Supplementary Files

This is a list of supplementary files associated with this preprint. Click to download.

- [SUPPLE1.mp4](#)
- [RevisedSupplementaryInformation.pdf](#)